

Layered Ruthenium Oxides: From Band Metal to Mott Insulator

A. V. Puchkov,¹ M. C. Schabel,¹ D. N. Basov,² T. Startseva,³ G. Cao,⁴ T. Timusk,³ and Z.-X. Shen¹

¹*Department of Applied Physics, Stanford University, Stanford, California 94305-4045*

²*Department of Physics, University of California at San Diego, La Jolla, California 92093-0319*

³*Department of Physics and Astronomy, McMaster University, Hamilton, Ontario, Canada L8S4M1*

⁴*National High Magnetic Field Laboratory, Florida State University, Tallahassee, Florida 32310*

(Received 12 February 1998)

We present results of the first optical and angle-resolved photoemission study on a layered ruthenium oxide system with various Ca/Sr substitution levels. Using two-plane $(\text{Sr}_{1-x}\text{Ca}_x)_3\text{Ru}_2\text{O}_7$ and one-plane Ca_2RuO_4 crystals we were able to study evolution of the electronic properties in a range from a band metal ($\text{Sr}_3\text{Ru}_2\text{O}_7$) to a “bad” metal ($\text{Ca}_3\text{Ru}_2\text{O}_7$) to a Mott-Hubbard insulator (Ca_2RuO_4). Apart from a Mott-Hubbard metal-insulator transition (MIT), we have uncovered a qualitative change of the electronic properties at a critical $x = 0.33$. We suggest that the latter is a result of a quantum phase transition into an antiferromagnetic phase that precedes the real Mott-Hubbard MIT. [S0031-9007(98)07196-8]

PACS numbers: 71.20.Eh, 71.27.+a, 71.30.+h, 79.60.-i

Perovskite ruthenium oxides of the Ruddlesden-Popper type, $(\text{Sr}/\text{Ca})_{n+1}\text{Ru}_n\text{O}_{3n+1}$, have attracted significant attention due, in part, to the recent discovery of superconductivity in $\text{Sr}_2\text{Ru}_4\text{O}_4$ (Sr214) [1]. In addition these materials exhibit a rich variety of magnetic phases [2–5], and bear strong structural resemblance to the cuprate superconductors, with RuO_2 planes taking the place of the CuO_2 planes. A controversy about a topology of Sr214 Fermi surface has increased the interest even further [6].

Since the discovery of high-temperature superconductivity in layered cuprates, understanding of Mott-Hubbard metal-insulator transition (MIT) in a quasi-two-dimensional (2D) system has been a subject of significant interest. In a simplest Mott-Hubbard description, a MIT is controlled by the relative magnitude of the on-site Coulomb interaction U and the one-electron bandwidth W . A splitting between the lower and upper Hubbard bands increases as U/W increases and for a half-filled band MIT occurs at $U/W \approx 1$, where a Mott-Hubbard gap opens. Interaction between magnetic moments at neighboring lattice sites favors antiferromagnetic (AFM) order in a Mott-Hubbard insulator. An AFM ground state has a higher degree of degeneracy than a nonmagnetic (or ferromagnetic) metallic since up and down directions of magnetic moment are not equivalent. Thus, AFM ground state contains a new property and cannot be transformed to a nonmagnetic (ferromagnetic) one without a ground state symmetry change. This implies that a zero-temperature, or quantum, phase transition (QPT) must occur as U/W is varied from zero to large values corresponding to an AFM insulator.

While Sr_2RuO_4 is a good metal and is believed to be well described within a framework of Fermi liquid theory, Ca_2RuO_4 is an insulator [2]. It was suggested that the MIT in $(\text{Sr}/\text{Ca})_2\text{RuO}_4$ [(Sr/Ca)214] is of the Mott-Hubbard type resulting from lattice distortions caused by the smaller size of the Ca^{2+} ion compared to the Sr^{2+} ion. In this scenario the lattice distortions

lead to a reduction of an electronic orbital overlap, similar to that observed in 3D RNiO_3 [7], thus reducing W . A similar effect is expected for $(\text{Sr}/\text{Ca})_3\text{Ru}_2\text{O}_7$ [(Sr/Ca)327], although the structural distortions and the corresponding bandwidth reduction may be smaller in this more rigid two-plane structure. Thus Sr/Ca substitution in layered $(\text{Sr}/\text{Ca})_{n+1}\text{Ru}_n\text{O}_{3n+1}$ ($n = 1, 2$) provides a way for a continuous “tuning” of Mott-Hubbard parameter U/W , making it an ideal system for an experimental study of a transition from normal metal to Mott insulator at a constant carrier doping in a quasi-2D system [2,8].

In this Letter, we report results of the first systematic study of the effect of Sr/Ca substitution on electronic properties of layered ruthenium oxides probed by optical and angle-resolved photoemission (ARPES) spectroscopies. Using two-plane (Sr/Ca)327 and one-plane Ca214 crystals we were able to span a wide range of electronic properties from band metal (Sr327) to Mott insulator (Ca214). A MIT was observed in the optical results and an on-site Coulomb interaction was estimated as 1.1–1.2 eV. A continuous loss of coherence, characteristic for a Mott-Hubbard system approaching MIT, was observed in (Sr/Ca)327 with increasing Ca concentration in both the optical and ARPES results. In addition to observing these changes, results of a detailed ARPES study indicate a qualitative change at $x \approx 0.33$. While at $x < 0.33$ the ARPES spectra are characterized by dispersive features crossing the Fermi energy, E_F , at $x \geq 0.33$ the ARPES features do not cross E_F . Considering results of previous magnetization experiments, which indicate emergence of in-plane AFM correlations at $x \approx 0.33$ [3], we suggest that the qualitative changes in the electronic properties of (Sr/Ca)327 at $x \approx 0.3$ –0.4 result from a QPT into an AFM phase, preceding the real Mott-Hubbard MIT. To the best of our knowledge, this detailed behavior has not been observed before.

Reflectivity measurements performed over the energy range from 6 meV to 4.3 eV (3 eV for Ca214) on as-grown

crystals were used to calculate the complex optical conductivity through Kramers-Kronig analysis. The single crystal samples formed platelets of $1 \times 1 \text{ mm}^2$ typical dimension in the ab plane. Details of the growth and preparation of crystals have been reported elsewhere [3,9]. An AFM ordering transition in our Ca214 samples was observed at $T_N = 110 \text{ K}$. For the ARPES experiments samples were cleaved *in situ* in vacuum better than 5×10^{-11} torr. The (Sr/Ca)327 crystals were cleaved and measured at $T = 20 \text{ K}$. Ca214 crystals were cleaved and measured at $T = 100 \text{ K}$. For $x = 0.58, 1$, and Ca214 we also performed ARPES measurements at $T > T_N$ and, on the energy scales discussed in this paper, the results were similar. Photons at $h\nu = 22.4 \text{ eV}$ and $h\nu = 27.4 \text{ eV}$ were generated on the undulator beam line 5-3 at Stanford Synchrotron Radiation Laboratory (SSRL). The instrumental energy resolution was 0.25 and 35 meV for the optical and ARPES experiments, respectively. At least three samples were measured for each composition (more for $x = 0, 1$) and the results were found to be consistent with each other. Prior to ARPES measurements samples were characterized and aligned using Laue diffraction. Sharp, dispersive valence band peaks as well as absence of well known contamination or a degradation derived feature at about 10 eV [10] speak for a good surface quality.

$\sigma_1(\omega)$, the real part of the optical conductivity, is plotted for Sr327, Ca327, and Ca214 in Fig. 1. The inter-band optical spectra for Ca327 and Sr327 are essentially identical, with a peak at around 3 eV. However, at low energies the spectra are qualitatively different. The low-energy $\sigma_1(\omega)$ of Sr327 is steeply increasing towards zero energy suggesting coherent charge transport. In a contrast

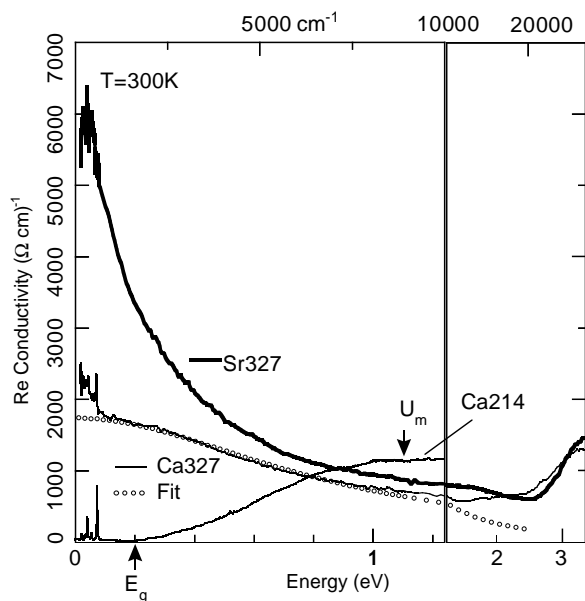


FIG. 1. The optical conductivities of Sr327, Ca327, and Ca214 taken at room temperature. Note a scale change at $\hbar\omega = 1.25 \text{ eV}$. A Lorentz oscillator fit to the high-energy $\sigma_1(\omega)$ for Ca327 is shown with the open circles. E_g is the optical gap and U_m is the on-site Coulomb energy for Ca214.

to Sr327, the optical conductivity of Ca327 is mostly composed of a single, very broad component that can be fitted to a broad Lorentzian, $\sigma_1(\omega) = \omega_p^2 \tau / [4\pi(1 + \omega^2 \tau^2)]$, where ω_p is the plasma frequency of the carriers and $1/\tau$ is their scattering rate. Adopting terminology from the high- T_c cuprates, we term this the midinfrared (MIR) band. We note that the MIR band is a universal signature of weakly doped Mott-Hubbard insulators, observed in the cuprates, nickelates, titanates, etc. [11]. Numerical values obtained from the fit are $\hbar\omega_p = 3.3 \text{ eV}$ and $\hbar/\tau = 0.84 \text{ eV}$. The large value of the scattering rate is indicative of an extremely short mean free path, l , for the carriers. Assuming a typical Fermi velocity of 10^7 – 10^8 cm/s , one finds $l = 0.8$ – 8 \AA , well below the limit for coherent, bandlike transport. A dc conductivity that can be extrapolated from the low-energy $\sigma_1(\omega)$ is just above the critical Mott conductivity $\sigma = e^2/3\hbar a = 2200 \text{ \Omega}^{-1} \text{ cm}^{-1}$, where $a = 3.84 \text{ \AA}$ is an in-plane lattice constant [4].

The optical conductivity of Ca214 is insulating, with a broad maximum at ~ 1.1 – 1.2 eV and an optical gap $E_g \approx 0.2 \text{ eV}$, which is in a good agreement with the activation energy of 0.2 eV found in dc resistivity measurements [2,9]. The sharp structure at low energies is due to phonons. The overall shape of the conductivity is very similar to that observed for a correlated insulator V_2O_3 [12] and predicted theoretically for a Mott-Hubbard insulator [13]. Using a one-band analysis similar to that employed in Ref. [12], we estimate an on-site Coulomb interaction from the position of the peak in $\sigma_1(\omega)$, $U_m \approx 1.1$ – 1.2 eV , and a single-particle bandwidth from the width of the peak, $D_m \approx 1 \text{ eV}$. A loss of coherence observed in a material sequence from Sr327 to Ca327 to Ca214 is remarkably similar to that observed previously in the doping-induced Mott transition study on the 3D $\text{La}_{1-x}\text{TiO}_3$ system [14].

While results of the optical measurements provide important information about MIT, it is of great interest to examine evolution of the electronic properties in even more detail using ARPES. Because of space limitations we present spectra only from a few \mathbf{k} points. Additional data taken over much more extensive \mathbf{k} grids validate the conclusions presented here. Energy distribution curve (EDC) spectra for (Sr/Ca)327 at normal emission [Γ , or $(k_x a, k_y a) = (0, 0)$, point] at various x are plotted in Figs. 2a and 2b at different energy scales. The spectra were normalized to the total integrated intensity in the 0–10 eV binding energy window. Equivalent data taken on a single layer Ca214 crystal at $T = 100 \text{ K}$ are shown by the dashed lines. The spectra are all qualitatively similar at binding energies above 2 eV, apart from a prominent feature at 7.5 eV in Ca327, which appears to evolve with increasing Ca concentration in (Sr/Ca)327. The similarity of the valence band electronic structure corroborates the high-energy optical spectra which also show little difference between Ca327 and Sr327.

The sharp feature lying near the Fermi energy in Sr327 exhibits behavior reminiscent to that of a surface-related feature observed in $\text{YBa}_2\text{Cu}_3\text{O}_{6.9}$ [15], including a strong

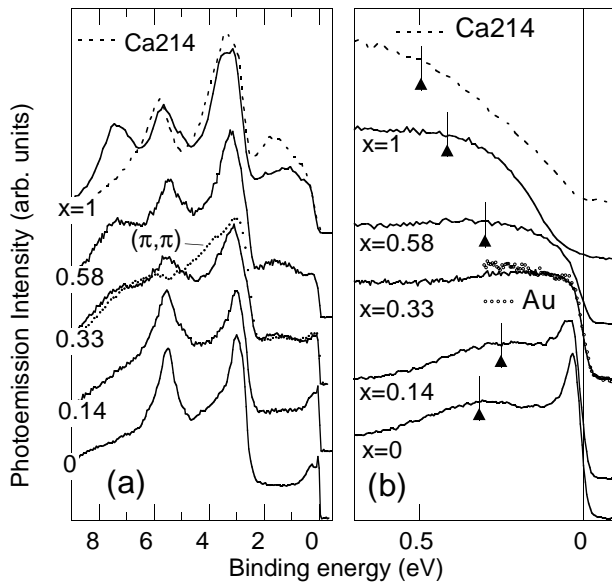


FIG. 2. ARPES spectra from $(\text{Ca}_x\text{Sr}_{1-x})_3\text{Ru}_2\text{O}_7$ and Ca214 (dashed lines), taken at the Γ point using $h\nu = 22.4$ eV. The dotted line in panel (a) for $x = 0.33$ is taken at X [or $(k_x a, k_y a) = (\pi, \pi)$] and demonstrates the dispersion in a valence band spectrum. In panel (b) a gold spectrum is shown by the open symbols superimposed on the $x = 0.33$ spectrum.

dependence on photon energy and a complete lack of measurable dispersion [16]. Also, its extreme narrowness is uncharacteristic of quasiparticles normally observed in correlated materials, hinting that this peak may be surface derived. As x is increased, the peak loses intensity without measurable changes in its binding energy. The feature centered at 350 meV at $x = 0$ shifts *towards* the Fermi energy and becomes notably broader with increasing x , as indicated by the arrows. However, at $x = 0.33$ this trend is reversed and the spectral weight starts moving *away* from the Fermi energy. It finally forms a broad feature centered at about ≈ 400 meV below E_F in Ca327. As a result, the spectral weight at the Fermi energy in Ca327 is very small, an observation confirmed by measurements throughout the Brillouin zone. As x increases beyond $x \approx 0.33$ another broad feature, centered at 1.2 eV for $x = 1$, appears at higher binding energies. For Ca214, ARPES intensity is characterized by a broad shoulder at 500 meV and a peak at 1.5 eV.

The angle-resolved spectra along the Γ - X [or $(k_x a, k_y a) = (0, 0) - (\pi, \pi)$] line for $(\text{Ca}/\text{Sr})_3\text{Ru}_2\text{O}_7$ at various x and Ca214 are shown in Fig. 3. In panel 3a, a comparatively broad peak lying about 350 meV below E_F at Γ shows clear dispersion along the Γ - X line and appears to correspond to the bottom of an upwardly dispersive conduction band. A second dispersive feature visible in Fig. 3a corresponds to a second conduction band centered at Γ . There exists a third dispersive feature in Sr327, not clearly visible in Fig. 3a but more pronounced in Fig. 3b and easily identifiable in spectra taken at a higher photon energy of $h\nu = 27.4$ eV (not

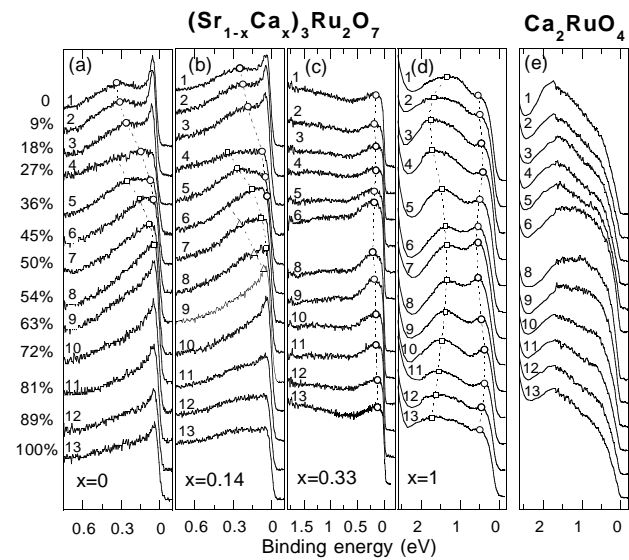


FIG. 3. The ARPES results for the members of $\text{Ca}_x\text{Sr}_{1-x}\text{Ru}_2\text{O}_7$ series along the Γ - X line using $h\nu = 22.4$ eV. Open symbols mark some of the dispersive features. Numbers on the left show position in \mathbf{k} space along the Γ - X line, starting at Γ . The 50% spectra for $x = 0.33$ and Ca214 are missing. Note a difference in energy scales.

shown). We note that a thorough investigation aimed at determining Fermi surface of Sr327 [16] produced results that are in a reasonable agreement with the band structure calculations for Sr327 [17]. In particular, in Sr327 we did not observe an extended Van Hove singularity (eVHs) at $(\pi, 0)$ [16] that led to a key discrepancy between results of ARPES and de Haas–Van Alphen experiments on the Sr214 system [6]. In fact, our recent ARPES experiments show no eVHs in Sr214 as well [18]. As Ca concentration is increased to $x = 0.33$ and above, the bandlike features disappear, blending into a single broad feature. In the $x = 1$ and $x = 0.58$ (not shown) materials both near 1.2 eV and near 0.5 eV features are weakly dispersive. It is difficult to identify dispersions in Ca214 although there is a redistribution of ARPES intensity along the Γ - X line. The origin of the 1.2–1.5 eV feature is not clear at the moment but we note that such multiple-peak structures are not uncommon in numerical calculations using the Hubbard model [19].

On the gray-scale plots in Figs. 4a–4c we show a second derivative of EDC spectra obtained along the Γ - X line. While we have used EDC's from Fig. 3 to obtain plots for $x = 0.33, 1$, data obtained at $h\nu = 27.4$ eV were used to obtain a plot for $x = 0$ in order to minimize the effect of the narrow feature close to E_F at Γ . At $x < 0.33$ we observe several [20] dispersive features crossing the Fermi energy, suggesting a bandlike electronic transport. Considering this together with the reasonable agreement obtained between the experimentally obtained Fermi surface of Sr327 and the one calculated within the one-electron approximation, we term $(\text{Sr}/\text{Ca})_3\text{Ru}_2\text{O}_7$ at $x < 0.33$ a “band metal.” Already at $x = 0.33$ the situation is different: the

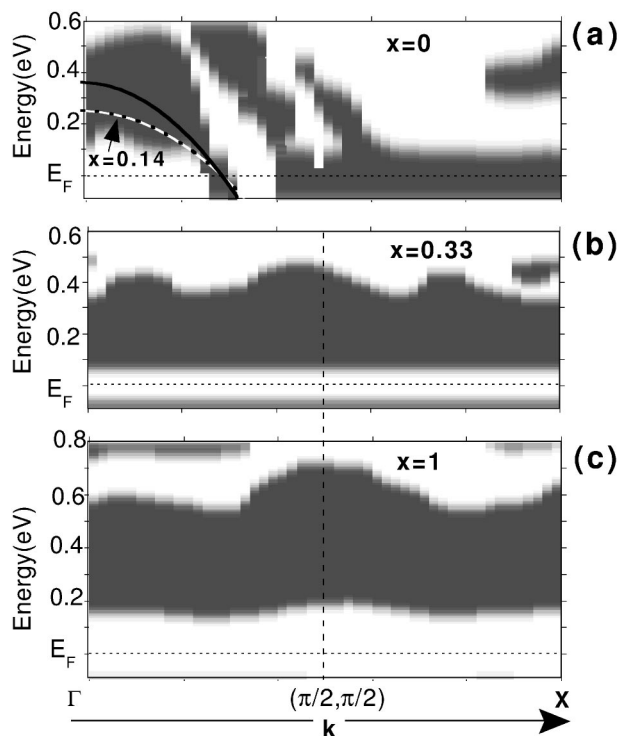


FIG. 4. Gray-scale plots of the second derivatives of EDC spectra along the Γ - X line. The gray scale is set up in such a way that the width of the features represents the width of the ARPES peaks. EDC curves from Fig. 3 were used for $x = 0.33, 1$ while data obtained at $h\nu = 27.4$ eV were used for $x = 0$. Solid and dashed lines in panel (a) show a fit to a parabolic $E(\mathbf{k})$ dependence as described in text.

dispersive features are replaced by a single, almost nondispersive band whose center of mass does not reach E_F . The low-binding energy edge of the broad band is still cut off by the Fermi function (Fig. 2b) so that the finite density of states at E_F is due to band broadness. Thus, the electronic transport is not bandlike but rather diffusive. We term the phase at $x \geq 0.33$ a “bad metal” phase. The lack of dispersion is clearly not a consequence of surface degradation since the main valence bands still show clear dispersion as a function of \mathbf{k} . As seen in Fig. 2a, the valence-band spectrum taken at X for $x = 0.33$, plotted with a dotted line, is clearly different from that taken at Γ . When x is increased above 0.33 correlation effects become stronger, shifting the ARPES spectral weight to higher binding energies. Similar behavior was observed previously in an angle-integrated photoemission study on $\text{Ca}_{1-x}\text{Sr}_x\text{VO}_3$ [21]. There is still, however, no gap in the optical spectra, and careful examination shows that ARPES intensity at E_F remains nonzero even for $x = 1$.

To quantify the changes observed we fitted a band closest to Γ at $x < 0.33$ with a parabola, $E(\mathbf{k}) = |\hbar\mathbf{k}|^2 / (2m^*) + a$, as shown by the solid and dashed lines in Fig. 4a for $x = 0, 0.14$, respectively. As x increases, m^* increases as well so that $m^*(x = 0.14)/m^*(x = 0) \approx 1.4$. Already at $x = 0.33$ the several distinct fast-

dispersing features disappear, blending into a single band close to E_F . While it is difficult to define m^* for $x = 0.33$, the overall lack of dispersion suggests it to be very large. As x approaches 1, dispersion strengthens again, suggesting lower m^* than at $x = 0.33$. All of the above indicates a criticality at $x \approx 0.3$. Emergence of an AFM order at $x \geq 0.33$, observed directly in magnetization experiments [3], demonstrates itself in the ARPES spectra which are clearly symmetrical with respect to the AFM Brillouin zone boundary at $(\pi/2, \pi/2)$. Considering the above, we suggest that our results, taken together with those of direct magnetic measurements [3], provide an evidence for a QPT between metallic and AFM phases at $x \approx 0.3$.

We acknowledge useful discussions with A. J. Berlinsky, J. E. Crow, M. Graiter, K. Kallin, R. B. Laughlin, and G. A. Sawatzky. SSRL is operated by the DOE office of Basic Energy Science, Division of Chemical Sciences. The Stanford work is also supported by the NSF Grants No. DMR-9311566 and No. DMR-9705210. The work at UCSD was supported by DOE under Contract No. DE-AC02-76CH00016 and A. F. Sloan Foundation. The work at McMaster University was supported by the Natural Science and Engineering Research Council and by the Canadian Institute for Advanced Research. The work at Florida State University was supported by NSF Cooperative Agreement No. DMR 95-27035 and the State of Florida.

- [1] Y. Maeno *et al.*, Nature (London) **372**, 532 (1994).
- [2] S. Nakatsuji *et al.*, J. Phys. Soc. Jpn. **66**, 1868 (1997).
- [3] G. Cao *et al.*, Phys. Rev. B **56**, 5387 (1997).
- [4] G. Cao *et al.*, Phys. Rev. Lett. **78**, 1751 (1997).
- [5] A. Kanbayasi *et al.*, J. Phys. Soc. Jpn. **41**, 1876 (1976).
- [6] T. Yokoya *et al.*, Phys. Rev. Lett. **78**, 2272 (1997); A. P. Mackenzie *et al.*, Phys. Rev. Lett. **78**, 2271 (1997).
- [7] J. B. Torrance *et al.*, Phys. Rev. B **45**, 8209 (1992).
- [8] Y. Maeno, Physica (Amsterdam) **282C–287C**, 206 (1997).
- [9] G. Cao *et al.*, Phys. Rev. B **56**, R2916 (1997).
- [10] A. Gulino *et al.*, Phys. Rev. B **51**, 6827 (1995).
- [11] S. Uchida *et al.*, Phys. Rev. B **43**, 7942 (1991); T. Katsufuji *et al.*, Phys. Rev. Lett. **75**, 3497 (1995); T. Katsufuji *et al.*, Phys. Rev. B **54**, R14230 (1996).
- [12] G. A. Thomas *et al.*, Phys. Rev. Lett. **73**, 1529 (1994).
- [13] R. Raimondi, Phys. Rev. B **51**, 10154 (1995).
- [14] D. A. Grandles *et al.*, Phys. Rev. B **49**, 16207 (1994).
- [15] M. C. Schabel *et al.*, Phys. Rev. B **57**, 6090 (1998).
- [16] A. V. Puchkov *et al.*, Phys. Rev. B **58**, 6671 (1998).
- [17] I. I. Mazin (private communication); I. Hase and Y. Nishihara, J. Phys. Soc. Jpn. **66**, 3517 (1997).
- [18] A. V. Puchkov *et al.* (unpublished).
- [19] E. Dagotto, Rev. Mod. Phys. **66**, 763 (1994).
- [20] While we resolve only three bands for Sr327 in Fig. 4, more careful examination yields more (Ref. [16]).
- [21] I. H. Inoue *et al.*, Phys. Rev. Lett. **74**, 2539 (1995).